Supplement of Atmos. Chem. Phys., 18, 16979–17001, 2018
https://doi.org/10.5194/acp-18-16979-2018-supplement

Atmospheric Chemistry and Physics
Open Access
EGU

Supplement of

Elucidating real-world vehicle emission factors from mobile measurements over a large metropolitan region: a focus on isocyanic acid, hydrogen cyanide, and black carbon

Sumi N. Wren et al.

Correspondence to: Sumi N. Wren (sumi.wren@gmail.com) and Jeffrey R. Brook (jeff.brook@utoronto.ca)

Supplementary Material

1. Additional materials and methods details

1.1. CRUISER driving routes

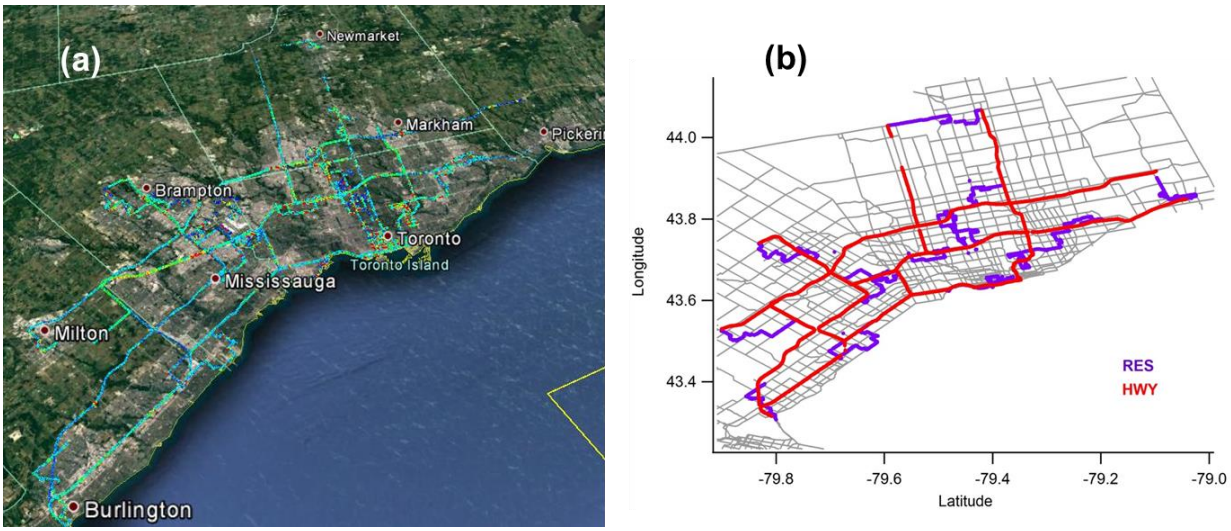

Figure S1. a) Map of summer and winter driving routes across the Greater Toronto Area (GTA). b) Map of summer and winter driving routes showing highways (red) and other road types (purple).

1.2. Algorithm for self-sampling

A two-stage algorithm was developed to flag periods that were likely impacted by CRUISER's own exhaust plume (COP). The first stage used relative wind speed and wind direction along with GPS speed-over-ground to identify periods of 'potential exhaust' (i.e., CRUISER moving slowly/stopped coincident with low wind speeds and/or wind moving in the direction of CRUISER's sampling inlets). The second stage of the COP algorithm identified periods of 'suspected exhaust' within the 'potential exhaust' windows during which exhaust tracers were found to co-vary above their background values (i.e., black carbon and NO for the Summer Campaign, fine particle counts and NO for the Winter Campaign). Periods of 'suspected exhaust' were removed from the data, along with those periods flagged as 'potential exhaust' for which exhaust tracer data was missing. The COP algorithm removed ~30% and ~20% of the 1 s pollutant data for the Summer and Winter Campaigns respectively.

1.3. PTR-TOF-MS: instrument details

Briefly, the instrument consists of four regions: a hollow cathode discharge ion source, a drift tube reaction chamber, a transfer lens system, and a reflectron time-of-flight (TOF) mass spectrometer. Reagent ions (H_3O^+) are generated from a stream of water vapour in the hollow cathode discharge and are directed towards the drift tube chamber, where the H_3O-VOC ion-molecule reactions take place. The sample containing the VOCs is continuously injected into the drift tube at a flow rate of 100 sccm and at temperature of 70°C. In this study, the drift tube pressure was maintained at 2.15 mbar and the electric field was maintained at 600 V difference.

The resulting E/N value was 140 Td. The protonated VOCs are directed by the transfer lens system to the pulse extraction region of the reflectron TOF mass spectrometer at a repetition rate of 1 Hz. The mass-to-charge ratios (m/z) of the ions are determined by the measured flight times, and an entire mass spectrum (m/z < 500) is generated with every pulse. In this study, the TOF mass spectrometer was operated in V-mode and maintained at a pressure of $<4 \times 10^{-7}$ mbar.

Air for analysis by the PTR-TOF-MS was sampled off the common gas phase inlet via a 2 m long PFA tube with 0.52 cm ID at a rate of 4.4 sLpm and the instrument sampled part of this flow (100 sccm) through a 120 cm insulated PEEK capillary with 0.08 cm ID heated to 70°C (hereafter the PTR-TOF-MS inlet). Background measurements were performed for 5 min every hour by passing the ambient air over a Pt catalytic convertor heated to 350 °C, which was housed in a home built zero/calibration unit (zero/cal unit) upstream of the PTR-TOF-MS inlet. A permeation tube containing trichlorobenzene ($Cl_3H_3C_6$) was connected at the front-end of the PTR-TOF-MS inlet to aid in mass calibration of the spectra.

The raw PTR-TOF mass spectra were analyzed using the Igor-based Tofware program (Tofwerk). The resolution of the instrument was approx. 4000 m/Δm. High-resolution (HR) fitting of the mass spectra provided signal intensity (in cps) for specific VOCs based on their exact mass.

The response of the PTR-TOF-MS to specific VOCs was determined using the zero/cal unit and a custom VOC gas standard (Ionicon) containing ca. 1 ppm each: acetonitrile, acetaldehyde, ethanol, acrolein, acetone, isoprene, benzene, methyl ethyl ketone (MEK), toluene, o-xylene and α-pinene. For each calibration, a small flow (0 – 20 sccm) of the standard was added to the inlet flow of zero air (ambient air passing the catalytic convertor) using the standard addition method. Sensitivities (a_i) in normalized counts per second (ncps) per ppbv were determined from these measurements by relating the known VOC mixing ratio to the detected signal intensity, as determined from the high-resolution fits (I_i). The response of the PTR-TOF-MS was found to be linear up to at least 20 ppbv for all of the VOCs. The volume mixing ratios in ppb were calculated according to:

$$VMR_i = \frac{1}{a_i}\left(\frac{I_i}{I_{21}} - \frac{I_{i,zero}}{I_{21,zero}}\right)\left(\frac{10^6}{500}\right)$$

The VOC signal intensity (I_i) was normalized to the signal of H_3O^{18+} at m/z 21.022 (I_{21}) and a correction for the normalized background signal was applied (denoted by subscript 'zero'). The third term in the equation accounts for a) the fact that the reagent ion signal of H_3O^{16+} is 500 times higher than that of H_3O^{18+} and b) the unit conversion to ppbv. Calibrations were performed before, during and after each campaign. The measured sensitivities deviated by <20% for all species; the reported sensitivities are the campaign averages. The detection limits were calculated as 2σ. Here σ represents the campaign average standard deviation of the zero measurement made during the routine calibrations. The sensitivities and detection limits are listed in Table S1. The sensitivities of the other C2 benzene species (m,p-xylene and ethylbenzene) are assumed to be the same as that of o-xylene.

Table S1. PTR-TOF-MS calibration sensitivities and detection limits for 1 s measurements

			Summer Campaign (July 2015)		Winter Campaign (Jan 2016)	
m/z	Species	Protonated Formula	Sensitivity, a_i (ncps ppbv^{-1})	Detection Limit (pptv)	Sensitivity, a_i (ncps ppbv^{-1})	Detection Limit (pptv)
79	Benzene	$C_6H_7^+$	8.9	110	10.9	155
93	Toluene	$C_7H_9^+$	9.7	125	12.7	240
107	o-xylene	$C_8H_{11}^+$	10.3	110	13.7	160

1.4. HR-TOF-CIMS: instrument details

The HR-TOF-CIMS sampled through (0.635 cm O.D., 0.580 cm ID., 3 m length) heated (50 °C) PFA (Teflon) inlet into the ion-molecule reaction (IMR) region of the CIMS via a critical orifice at 1.7 L min^{-1}. The CIMS subsampled from a bypass flow of ~22 sLpm to reduce the residence time in the inlet. The IMR pressure was maintained at 100 mbar. Iodide ions were generated by passing a stream of methyl iodide (from a permeation device) in N_2 past a ^{210}Po radioactive source. The ion-molecule reaction occurs via an adduct reaction:

$$I^-\cdot(H_2O)+X\rightarrow X\cdot I^-+H_2O$$

which allows HNCO to be detected as HNCO·I$^-$ (*m/z* = 170) and HCN to be detected as HCN·I$^-$ (*m/z* = 154).

Background measurements were performed once per hour for a duration of 5 min, by diverting the ambient air through a pair of acidic gas traps. The traps were comprised of nylon wool coated in a saturated solution of sodium bicarbonate, followed by activated carbon. A constant flow of 1 mL min^{-1} of isotopically labelled propionic acid (^{13}C) was introduced into the HR-TOF-CIMS during all sampling and calibrations to correct for dynamic fluctuations in the response factors.

The raw HR-TOF-CIMS mass spectra were analyzed using the Igor-based Tofware program (Tofwerk). The reagent iodide ion signal was approximately 1 × 10^6 cps and was used to normalized the analyte signals. The mass resolution of the instrument was approx. 5000 m/Δm for ions spanning m/z = 100 to greater than m/z = 200.

Calibrations of HNCO were conducted by thermally decomposing cyanuric acid at 250 °C to HNCO in a heater (Roberts et al., 2010); the diffusion rate was quantified via Fourier Transform Infrared Spectroscopy (FTIR; Thermo-Fisher Inc.) Calibrations of HCN were performed by diluting a HCN gas standard (Air Liquide, ppmv in N_2) in zero air. Humidity dependant response factors were derived by diluting the calibration gas flows with humidified air to a final RH ranging from ~9% to 90%.For these HR-TOF-CIMS measurements the humidity entering the ion-molecule region (IMR) is proportional to the m/z fragment ratios associated with iodide (I^-; m/z 127) and iodide clustered with water ($I\cdot H_2O^-$; m/z 145). Hence the ratio of m/z 127: m/z 145 during humidity calibrations is applied to the ambient data based upon the ambient m/z 127: m/z 145 ratio. The magnitude of the humidity corrections based upon the above ratio during the study ranged from 10 - 20% for both HNCO and HCN. Calibrations (relative to the internal standard) were performed before and after the Summer and Winter Campaigns. Detection limits (2σ) for HNCO and HCN were estimated to be 7 pptv each.

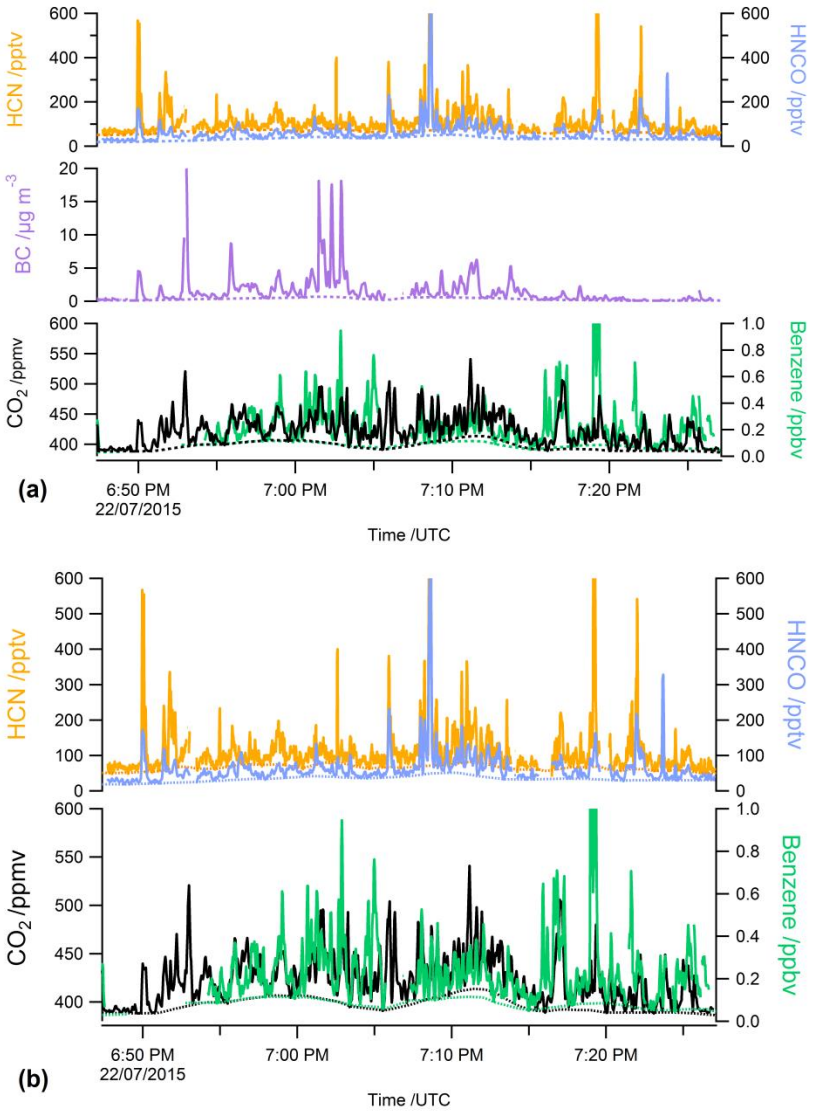

Figure S2. Sample pollutant time series for (a) the Summer Campaign and (b) the Winter Campaign. Smoothed pollutant data (solid lines) and calculated baseline (dashed lines). HCN (left axis, yellow), HNCO (right axis, blue), BC (left axis, purple), CO2 (left axis, black), Benzene (right axis, green).

1.5. Plume-Based emission factor algorithm

The plume-based emission factor algorithm was run separately for each day of driving for pollutants sharing a common inlet with CO_2. The daily pollutant data was first averaged to 2 s to match the time resolution of the CO_2 data. Boxcar smoothing of 3 points (5 seconds) was then applied to both the pollutant and CO_2 data to reduce noise. A time offset was applied to the pollutant time series by visually optimizing the overlap between the two sets of data.

Baselines were calculated for both the CO_2 and pollutant time series from the smoothed data (following the approach of Larson et al. (Larson et al., 2017)). The baseline was calculated as

the rolling 2nd percentile over a 90 point (180 s = 3 min) window. Due to the initial smoothing of the time series, we found that the resulting baseline is similar to the one calculated as the rolling 5th percentile for the un-smoothed data over the same window. Boxcar smoothing was then applied over a 90 point (180 s = 3 min) window for both time series.

Two types of plumes were then identified: single peak plumes and multi-peak plumes. Single peak plumes (SPP) are plumes containing a single CO_2 peak, with CO_2 concentrations returning to within 2% of the baseline at the peak boundaries (henceforth the 'baseline threshold'). Multi-peak plumes (MPP) are plumes containing one or more peaks, with the local minimum between peaks not returning to below the baseline threshold (this set contains the SPP set). This allowed overlapping/unresolved peaks to be counted as a single plume. An example of the plume capture is shown in Fig. S3.

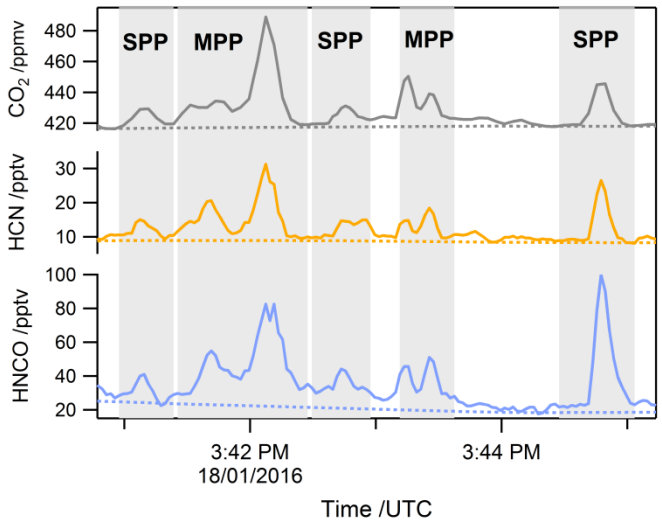

Figure S3. An example of plume capture. Top panel: CO_2 (grey), middle panel: HCN (yellow), bottom panel: HNCO (blue). The solid line shows the smoothed pollutant concentration (before background correction), the dotted line shows the calculated baseline. The shaded regions indicate the plume boundaries and are designated as SPP (single-peak plume) or MPP (multi-peak plume).

The first derivative of the CO_2 time series was obtained and then further smoothed (boxcar of 3 points/5 seconds). Peak start times (left boundaries) were identified by the instances when the first derivative crossed zero from low to high. Peak locations (maxima) were identified by the instances when the first derivative crossed zero from high to low. Peaks were then rejected if the first derivative of the peak leading edge did not meet a user-defined threshold of 0.5. This threshold (henceforth the 'derivative threshold') was set in order to ensure that only significant peaks were identified, and that small fluctuations were not counted in the analysis. Peak end times (right boundaries) were identified in a similar manner.

Plumes were further filtered to remove plumes that were < 10 s in duration and with an average CO_2 response < 5 ppmv s^{-1} above baseline over the integration period. For the Summer Campaign, filtering based on plume duration led the removal of ca. 50 single-peak plumes with very little effect on the average or median emission factors. The average and median emission factors

were more sensitive to the choice of CO_2 removal criteria. Removal of peaks based on various thresholds for average CO_2 response (> 3, 5, 8, 10 ppmv s^{-1}) or maximum CO_2 response (> 10, 20, 30, 40 ppmv) over the integrations period was explored. Generally it was found that tightening the constraints led to a reduction in the median and mean EFs with a concomitant decrease in the number of plumes remaining in the analysis. For benzene EFs calculated from single peak plumes, the 5 ppmv s^{-1} average CO_2 threshold led to a 15% reduction in median EF and a 28% reduction in the total number of plumes. Under these conditions, the benzene median and mean EF calculated using all plumes (MPP) was within 15% of that calculated using single peak plumes (SPP). Increasing the threshold to 8 ppmv s^{-1} reduced the median EF by only 13% but reduced the number of plumes by 39%. Decreasing the threshold from 5 ppmv s^{-1} to 3 ppmv s^{-1} increased the median EF by 13% and the number of plumes by 29%. The 5 ppmv s^{-1} average CO_2 threshold resulted in similar statistics for the EFs and the number of plumes as the 20 ppmv maximum CO_2 threshold. Although other groups (Jiang et al., 2005;Park et al., 2011) have used stricter constraints (e.g. 40 ppmv maximum CO_2), the 5 ppmv s^{-1} threshold provided a good balance between preserving a large number of plumes while ensuring that captured plumes were not erroneous. Wang et al. (2015) also used an average CO_2 response of 5 ppmv s^{-1}. We note that Wang et al. (2015) performed extensive sensitivity tests on the influence of plume definition on mean EFs.

Baseline calculation has been identified by others (Park et al., 2011) as the source of greatest uncertainty for the EF calculation. The sensitivity of the calculated emission factors to the choice of baseline was investigated on EFs calculated prior to any filtering. We found that using a rolling 5^{th} percentile instead of rolling 2^{nd} percentile reduced the benzene median EF by ca. 7% for both the SPP and MPP cases. Using a window of 45 pnts (90 s), 150 pnts (300 s), or 300 pnts (600s) resulted in changes to the benzene median EF of <2.5% for both the SPP and MPP cases.

For the Summer Campaign, focusing on the target BTEX species, a number of exceptionally high emission factors in the post-filtering dataset were identified and the pollutant and CO_2 time-series of their corresponding plumes were visually inspected (the entire MPP set). These high EFs were characterized as being > 500 mg kg_{fuel}^{-1} for benzene and >1000 mg kg_{fuel}^{-1} for both toluene and C2 benzenes, or roughly an order of magnitude greater than their respective median EFs. Upon visual inspection, it was found that 30 out of the 40 identified high EF plumes were very clearly erroneously captured (poor overlap of pollutant plume and CO_2 plume). A final EF dataset was created by removing these plumes from the EF calculation for all Summer Campaign species. Note that 23 out of 30 of these erroneous plumes were SPP plumes, representing only 4% of the post-filtering SPP dataset. The 30 erroneous plumes represented only 3% of the post-filtering MPP dataset. Removal of these plumes resulted in large decrease in the average EFs (20 – 50% for the target species benzene, toluene, and C2 benzene) with respect to the post-filtering dataset, but only a small decrease (< 4%) in the median EFs.

For the Winter Campaign, plumes giving rise to HNCO EFs above 20 mg kg_{fuel}^{-1} and HCN EFs above 10 mg kg_{fuel}^{-1} were inspected. Of the 16 high EF plumes identified for HNCO, six were deemed erroneous and of the four high EF plumes identified for HCN, only on was deemed to be erroneous (and was one of the six found for HNCO). Of these erroneous plumes, all but one were single peak

plumes (SPP). The erroneous plumes (<1% of the data) were removed from both the HNCO and HCN post-filtering datasets to create the final datasets.

Table S2. Plume statistics for the Summer Campaign (benzene). Note that the statistics may be slightly different for other pollutants (due to missing data, different zero periods etc.).

	Single Peak Plumes (SPP)	Multi-peak Plumes (MPP)
Number Driving Days	**9**	**9**
Before Filtering		
Number Plumes	952	1274
Mean Time Per Plume /s	19	34
Median Time Per Plume /s	16	20
Average Number Peaks Per Plume	NA	1.7
Post-Filtering (10 s plume duration, 5 ppmv CO_2)		
Number Plumes	650	970
Mean Time Per Plume /s	21	39
Median Time Per Plume /s	18	24
Average Number Peaks Per Plume	NA	1.9
Mean Plume-averaged CO_2 Response/ppmv s^{-1}	11.1±6.5	15.4±10.2
Mean Plume-Integrated CO_2 response	258±255	892±1666
After Removal Erroneous Plumes		
Number Plumes	627	940
Mean Time Per Plume /s	21	40
Median Time Per Plume /s	18	24
Average Number Peaks Per Plume	NA	2.0
Mean Plume-averaged CO_2 Response/ppmv s^{-1}	11.1±6.4	15.4±10.2
Mean Plume-Integrated CO_2 response	255±249	906±1688

Table S3. Plume statistics for the Winter Campaign (HNCO, HCN)

	Single Peak Plumes (SPP)	Multi-peak Plumes (MPP)
Number Driving Days	**8**	**8**
Before Filtering		
Number Plumes	1382	1743
Mean Time Per Plume /s	24	39
Median Time Per Plume /s	20	22
Average Number Peaks Per Plume	NA	1.5
Post-Filtering (10 s plume duration, 5 ppmv CO_2)		
Number Plumes	1019	1378
Mean Time Per Plumes /s	25	44
Median Time Per Plume /s	22	26
Average Number Peaks Per Plume	NA	1.7
Mean Plume-averaged CO_2 Response/ppmv s^{-1}	9.9±6.2	13.0±9.1
Mean Plume-Integrated CO_2 response	277±319	832±1545
After Removal Erroneous Plumes		
Number Plumes	1014	1372
Mean Time Per Plumes /s	26	44
Median Time Per Plume /s	22	26
Average Number Peaks Per Plume	NA	1.7
Mean Plume-averaged CO_2 Response/ppmv s^{-1}	9.9±6.2	13.0±9.1
Mean Plume-Integrated CO_2 response	278±320	832±1544

2. Background and local pollutant contributions

Table S4. Mean daytime pollutant concentrations as a function of regional (background) vs. local (on-road) contribution.

	Benzene		BC	HNCO		HCN	
	Summer	Winter	Summer	Summer	Winter	Summer	Winter
Road Type	Mean (±1σ) pptv	Mean (±1σ) pptv	Mean (±1σ) μg m^{-3}	Mean (±1σ) pptv	Mean (±1σ) pptv	Mean (±1σ) pptv	Mean (±1σ) pptv
BKG	93±62	115±62	0.30±0.48	29±13	10.7±8.2	40±20	5.8±3.0
LOCAL	159±313	195±240	0.84±2.32	17±31	15.3±48.4	25±42	5.0±12.6

BKG = background contribution, LOCAL = local contribution (above-background)

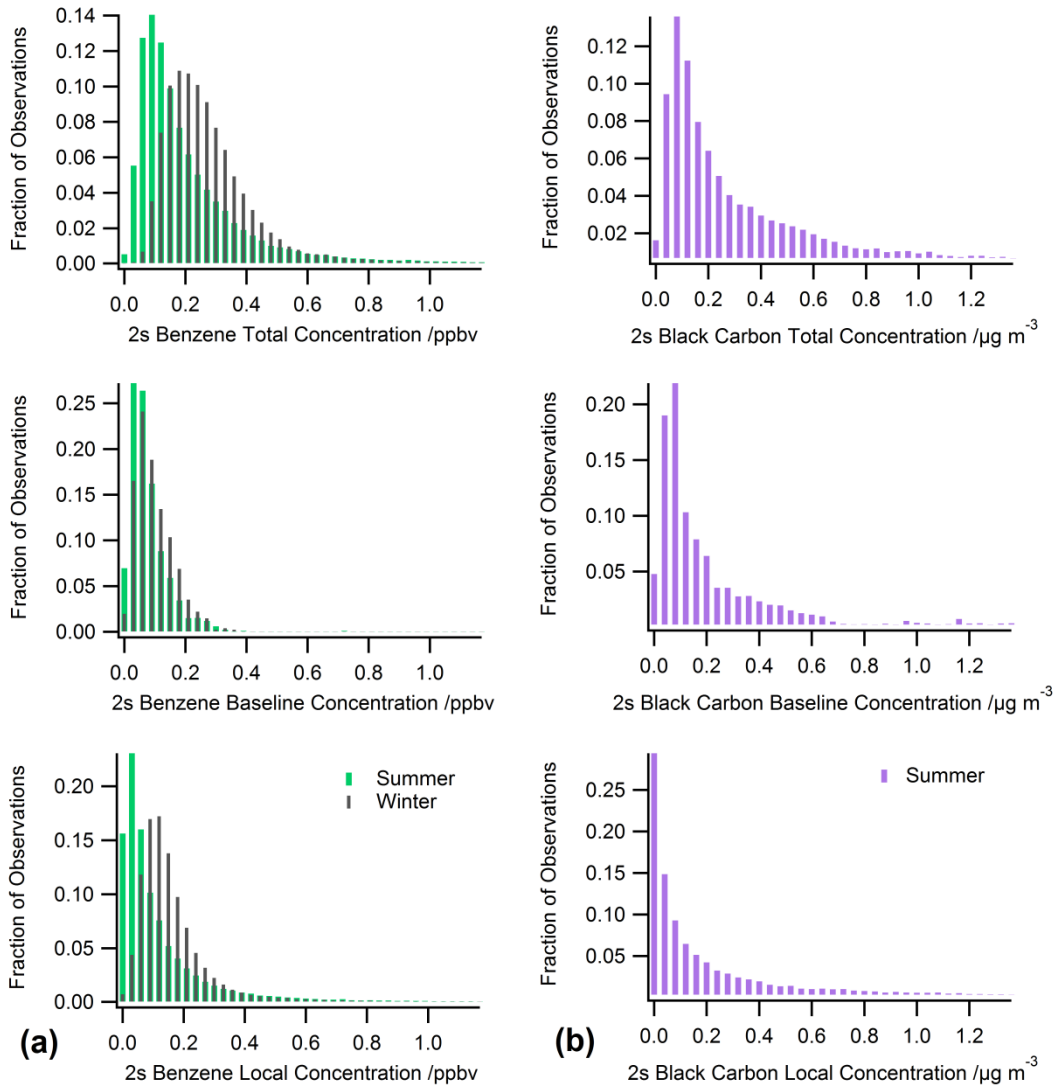

Figure S4. Distribution of ambient mixing ratios for a) benzene and b) black carbon. Top panel: total concentration. Middle panel: baseline (BKG) concentration. Bottom panel: background-corrected (LOCAL) concentration. Summer Campaign (July 2015) shown as colored bars, Winter Campaign (Jan 2016) shown as grey bars.

3. Emission factor methodologies: results

3.1. Plume-based emission factor methodology

Plume-based median, mean, and interquartile range (IQR) single-peak plume (SPP) EFs for a number of traffic pollutants are listed in Table 2. Results for the multi-peak plumes (MPP) are summarized in Table S6. The distribution histograms of plume-based EFs are shown in Fig. 3 for benzene, BC, HNCO, and HCN and in Fig. S5 for others traffic pollutants (toluene, C2 benzenes, NO, NO_2, NO_x, and PN).The mean MPP EFs are similar but consistently lower than the corresponding SPP EFs (by up to 20 % depending on the pollutant). The median EFs for the MPP dataset are lower than the median EFs for the SPP dataset by only 2-13% depending on the pollutant. The IQRs for the MPP dataset are also narrower, likely due to the greater number of plumes in the analysis

Table S5. Plume-based median and mean emission factors calculated from multi-peak plumes (MPP) for the Summer and Winter Campaigns. Interquartile range (25^{th} – 75^{th} percentile) shown in brackets. Units for numerator given in the pollutant column, units for denominator given in the header.

Pollutant and Units	MPP $/kg_{fuel}^{-1}$
SUMMER	
Benzene */mg*	**42.9, 60.3** (28.4-68.1)
Toluene */mg*	**96.9, 162.0** (57.2-175.0)
C2 Benzenes[c] */mg*	**72.4, 129.9** (43.3-127.6)
NO_2 */g*	**1117, 1337** (623, 1676)
NO */g*	**1147, 1879** (623-1676)
NO_x (=NO + NO_2) */g*	**2305, 3210** (1267-4141)
Particle Counts $/10^{14}$ #	**9.0, 16.4** (4.3-20.0)
Black Carbon */mg*	**27.3, 80.2** (11.7-79.0)
WINTER	
HNCO */mg*	**2.15, 3.17** (1.27-3.81)
HCN */mg*	**0.50, 0.77** (0.02-0.06)

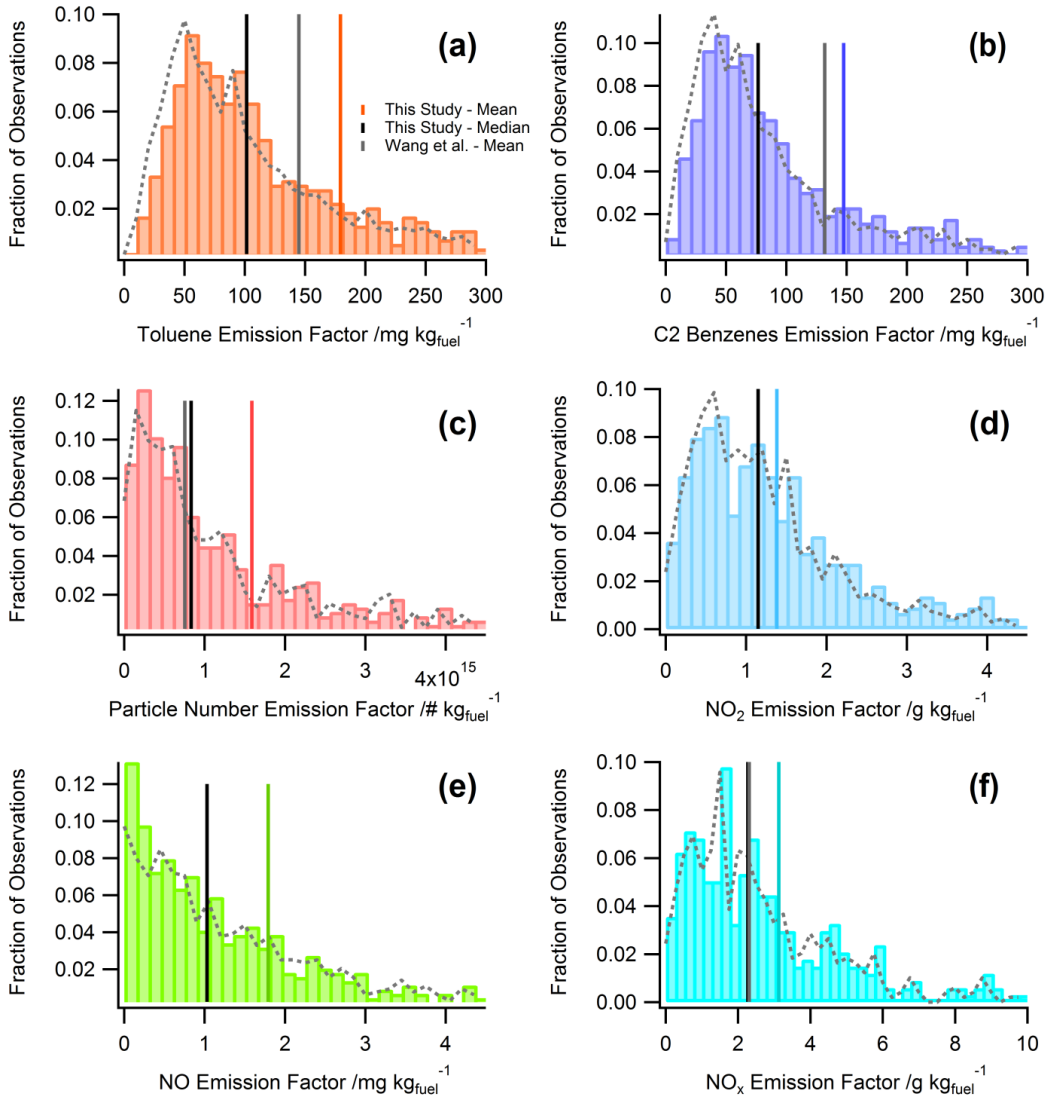

Figure S5. Plume-based emission factors obtained by CRUISER for (a) toluene, (b) C2 Benzenes (sum m-, p-, o-xylene and ethylbenzene) (c) particle number density (d) NO_2, (e) NO, and (f) NO_x for the SPP case (colored bars) and the MPP case (grey, dashed line). The median and mean EF values are indicated by the vertical black and colored lines respectively. Where available, the mean EF obtained by Wang et al. (2015) is indicated by the vertical grey line.

3.2. Time-based emission factor methodology

The mean and median EFs calculated using the time-based methodology and various integration periods are listed in Table S6 for both seasons for benzene, HNCO, and HCN, and in Table S7 for the summer for toluene, C2 benzenes, NO, NO_2, NO_x, PN, and BC.

The sensitivity of the mean and median EFs calculated using the time-based approach was investigated for summer benzene and summer HCN data and an interval of 120 s. The impact of the background definition on the median emission factors is shown below in Table S8. Overall it can be seen that a background that is more sensitive to fluctuations in concentration (i.e., case B3) or to the lowest concentrations (i.e., case B5) results in a larger median emission factor. However,

relative to the base scenario used in this study, changes to the median EF due to changes in the background definition are ultimately small (< 5%).

As was observed for the plume-based approach, the time-based mean EFs are consistently higher than the corresponding median EFs. The magnitude of the mean EF and its associated error are found to decrease with increasing integration period. The median EFs are found to be less sensitive to integration period and exhibit different trends depending on the pollutant identity. An integration period of 120 s was found to yield median EFs in closest agreement with the plume-based SPP median EFs for benzene, HNCO, and HCN, and so was used in all further discussion.

Table S6. Fuel-based median and mean (±1σ) emission factors calculated using the time-based approach and integration periods of 30, 60, 90 and 120 s for benzene, HNCO, and HCN. The number of periods (n) included in each calculation is shown in brackets. The median and mean EFs from the plume-based approach are shown in the first row (SPP) and second row (MPP) where available.

	Benzene /mg kg_{fuel}^{-1}		HNCO /mg kg_{fuel}^{-1}		HCN /mg kg_{fuel}^{-1}	
Season	Summer	Winter	Summer	Winter	Summer	Winter
SPP	**47.2**, 68.2	NA	NA	**2.25,** 3.30	NA	**0.52**, 0.82
MPP	**42.9**, 60.3	NA	NA	**2.15**, 3.17	NA	**0.50**, 0.77
30 s	**50.6**, 97.6±200 n=2930	**101.8**, 224±536 n=4034	**3.3**, 7.7±15.0 n=2604	**2.6**, 4.8±9.4 n=4141	**2.9**, 6.9±16.0 n=2605	**0.6**, 1.1±1.9 n=4141
60 s	**51.4**, 86.4±167 n=1465	**95.8**, 176±292 n=2017	**3.2**, 6.3±10.1 n=1302	**2.6**, 4.3±7.6 n=2070	**2.8**, 5.7±11.7 n=1302	**0.6**, 1.0±1.3 n=2070
90 s	**50.9**, 81.8±158 n=976	**93.5**, 154±200 n=1344	**3.1**, 5.6±7.4 n=868	**2.6**, 4.1±2.6 n=1380	**2.8**, 5.1±7.7 n=868	**0.6**, 0.9±1.0 n=1380
120 s	**50.2**, 79.5±142 n=732	**88.6**, 145±194 n=1008	**3.1**, 5.4±6.9 n=651	**2.6**, 4.0±5.5 n=1035	**2.7**, 4.8±7.6 n=651	**0.6**, 0.9±0.9 n=1035
Fractional difference[a]	**0.06**	NA	NA	**0.16**	NA	**0.15**

[a]Fractional difference time-based (120 s) EF vs plume-based (SPP) EF

Table S7. Fuel-based median and mean (±1σ) emission factors calculated using the time-based approach and integration periods of 30, 60, 90 and 120 s. The number of periods (n) included in each calculation is shown in brackets. The median and mean EFs from the plume-based approach are shown in the first row (SPP) and second row (MPP).

Season	Black Carbon /mg kg_{fuel}^{-1} Summer	NO /g kg_{fuel}^{-1} Summer	NO2 /g kg_{fuel}^{-1} Summer	Toluene /mg kg_{fuel}^{-1} Summer	Xylene /mg kg_{fuel}^{-1} Summer	PN /10^{14} # kg_{fuel}^{-1} Summer
SPP	**24.9**, 85.6	**1.0**, 1.8	**1.2**, 1.4	**101.6**, 179.5	**76.8**, 147.6	**8.3**, 15.9
MPP	**27.3**, 80.2	1.1, 1.9	**1.1**, 1.3	**96.9**, 162.0	**72.4**, 129.9	**9.0**, 16.4
30 s	**42.4**, 115 ± 390 n=2603	**1.4**, 2.5 ± 5.3 n=2651	**1.3**, 1.7 ± 1.6 n=2534	**118**, 338 ± 1059 n=2989	**87.9**, 300 ± 2072 n=2930	**10.6**, 22.6 ± 66.9 n=2593
60 s	**45.7**, 101 ± 210 n=1301	**1.6**, 2.4 ± 2.6 n=1325	**1.3**, 1.6 ± 1.2 n=1267	**120**, 294 ± 749 n=1494	**89.1**, 266 ± 1870 n=1465	**9.3**, 39.0 ± 116 n=1267
90 s	**51.0**, 96 ± 164 n=867	**1.7**, 2.4 ± 2.3 n=883	**1.3**, 1.5 ± 1.1 n=844	**124**, 273 ± 618 n=996	**93.0**, 258 ± 1861 n=976	**10.6**, 19.6 ± 40.5 n=864
120 s	**51.0**, 94 ± 148 n=650	**1.8**, 2.4 ± 2.1 n=662	**1.3**, 1.5 ± 1.0 n=633	**124**, 260 ± 495 n=747	**94.9**, 251 ± 1672 n=732	**10.5**, 18.2 ±27.5 n=648
Fractional difference[a]	**1.05**	**0.80**	**0.08**	**0.22**	**0.24**	**0.27**

[a]Fractional difference time-based (120 s) EF vs plume-based (SPP) EF

Table S8. Sensitivity of median emission factors calculated using the time-based approach to background calculation criteria.

	Background Case	Percentile	Rolling percentile window (s)	Additional boxcar smoothing (s)	Benzene Summer % Change to Median EF	HCN Summer % Change to Median EF
B1	Base	2	180	180	0	0
B2	Increased percentile	5	180	180	-1.9	-5.5
B3	Decreased window	2	60	60	+3.1	+2.0
B4	Increased window	2	360	360	-1.9	-3.6
B5	Decreased percentile	1	180	180	+2.4	+2.8

3.3. Plume-based vs. time-based methodologies

The plume-based SPP and MPP EFs are also included in Tables S7 and S8 for comparison with the time-based EFs. For all pollutants, the time-based approach consistently yields higher median EFs than the plume-based approach. However, the bias was found to be relatively small (< 25%) for all pollutants (benzene, toluene, C2 benzenes, NO_2, NO_x, PN) except NO (80% higher) and BC (>100% higher). The poor performance of the time-based method for NO and BC is likely related to the fact that the main emitters of these compounds are HDDV emissions, which leads to highly skewed plume-based EF distributions across the whole fleet. Distribution histograms of EFs obtained for summer NO and BC are displayed in Fig. S6 and show that the time-based EF distributions are weighted towards higher EFs (fewer counts of the lowest EFs). The discrepancy between plume-based and time-based NO EFs may also be related to the fact that NO is relatively short-lived (some tailpipe NO will be converted to NO_2) and it not known to which extent this chemical transformation is captured by the measurements.

There are a few possible reasons why the time-based methodology yields higher EFs for all other pollutants. First, the lower values for the plume-based approach may be attributed to the removal of 'erroneous' high-EF plumes. No similar attempt was made to identify and remove possible non-road contributions for the time-based calculations. Secondly, inclusion of periods with low above-background CO_2 levels (i.e., leading to a small denominator in EQ1) could potentially bias results high.

The ability of the time-based methodology to respond to trends in emission factors was evaluated by comparing the daily EFs calculated using the time-based methodology (120 s integration period) to those calculated using the plume-based methodology (SPP). This comparison is shown in Fig. S7 for summer benzene, winter HNCO, and winter HCN. As can be seen by Fig. S7, the daily trend in EFs is only captured ~ 75% of the time by the time-based approach for benzene, possibly due to the fact that non-vehicle emissions of benzene are included in the time-based calculation. However, the daily trend in is captured well for HNCO and HCN, pollutants with no other significant local sources.

The time-based methodology was developed here with the goal of obtaining EFs for pollutants not sharing a common inlet with CO_2 (thereby enabling the acquisition of seasonal EFs for HNCO and HCN). Benzene is known to have a higher EFs in the winter due to enhanced cold-start emissions and changes in fuel formulation (Lough et al., 2005)(McMaster Research). The time-

based approach effectively captures the factor of 2 greater wintertime EFs for benzene, giving confidence in the ability of this methodology to identify seasonal trends in emissions.

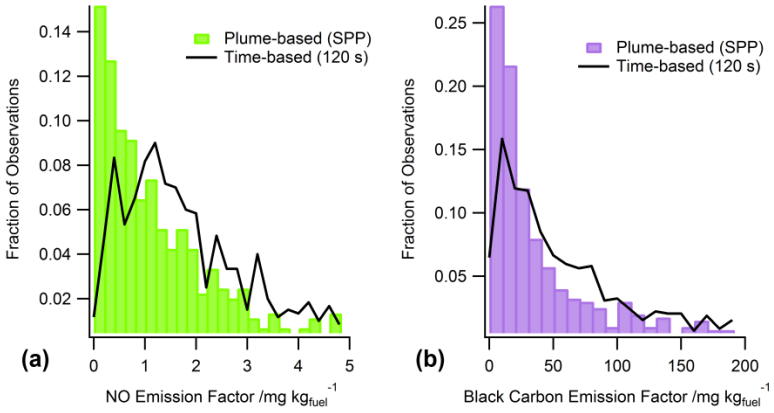

Figure S6. Distribution of emission factors obtained by the plume-based (SPP) approach (coloured bars) and time-based (120 s integration period) approach (black line) for a) summer NO (green) and b) summer BC (purple).

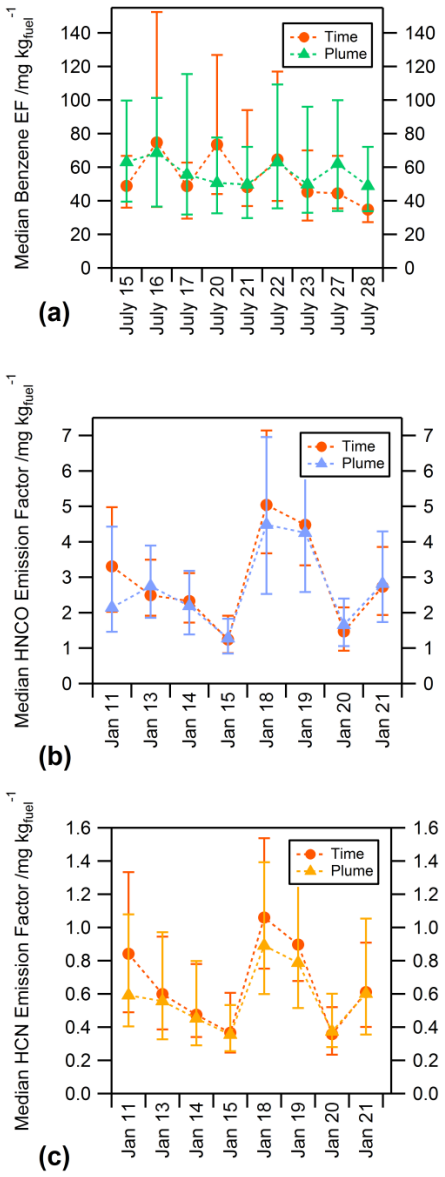

Figure S7. Daily median emission factors calculated using the time-based (120 s integration period) approach (orange circles) and plume-based (SPP) approach (colored triangles) for a) summer benzene (green), b) winter HNCO (blue), and c) winter HCN (yellow). The vertical error bars show the interquartile range for both measurements.

4. Black Carbon Emission Factors

Table S9. Comparison of literature black carbon (BC) emission factors from tunnel, near-road, and mobile studies in fuel-based units (mg kg_{fuel}^{-1}).

Reference	Type of study	BC detection	Average /mg kg_{fuel}^{-1}	Description of vehicles
This study	Mobile	HS-LII	24.9, 85.6[a] (mixed)	GTA fleet, 650 vehicle plumes
(Miguel et al., 1998)	Tunnel	PM1.3 and PM2.5 filter samples	30±2 (LDGV) 1440±160 (HDDV)	Caldecott Tunnel, CA, 1996
(Kirchstetter et al., 1999)	Tunnel	Aethelometer, 5 s	35±3 (LDGV) 1300±300 (HDDV)	Caldecott Tunnel, CA, 1997
(Jiang et al., 2005)	Mobile, catch-all	Aethelometer, 1 min	270±0.59 (mixed)	Mexico City fleet, 2003
(Ban-Weiss et al., 2008)	Tunnel	Aethelometer (Aeth) Filter (TOA)	26±4 (LDGV, Aeth) 22±4 (LDGV, TOA) 920±70 (HDDV, Aeth) 860±70(HDDV, TOA)	Caldecott Tunnel, CA, 2006
(Westerdahl et al., 2009)	Stationary roadside, mobile catch-all	Aethelometer, 1 min	300 (LDGV) 1300 (HDDV)	On-road fleet (Beijing, China, 2007)
(Park et al., 2011)	Mobile, vehicle chase	Aethelometer, 1 min	60 (LDGV) 500 (HDDV)	Wilmington, CA fleet, 2007 (93 HDDVs, 143 LDGVs)
(Hudda et al., 2013)	Mobile, catch-all (10 s road segments)	Aethelometer,	70±50 (LDGV) (410±210) - (1330±330) (HDDV)	Los Angeles freeways, CA
(Liggio et al., 2012)	Mobile, transect driving, and vehicle chase	Single-particle soot photometer (SP2), High-sensitivity laser-induced incandescence (HS-LII), 1 s	59.3, 151.8[a] (HS-LII – transect, mixed) 29.4, 71.2[a] (SP2 – transect, mixed) 152.7, 511.6[a] (HS-LII – HDDV chase) 115±80 (LDGV, reconstructed)	Toronto, 2010 (30 HDDV for chase events, 23 hours for transect driving)
(Dallmann et al., 2012)	Tunnel	Aethelometer, photoacoustic spectrometer, multi-angle absorption photometer (MAAP), 1 s	540±70 (HDDV, aethelometer) 580±90 (HDDV, photoacoustic) 590±110 (HDDV, MAAP)	Caldecott Tunnel, CA, 2010 (445 - 667 HDDV successfully captured)
(Dallmann et al., 2013)	Tunnel, with vehicle count apportionment	Aethelometer, 1 s	10±2 (LDGV)	Caldecott Tunnel, CA, 2010
(Wang et al., 2015)	Stationary near-road	Photoacoustic soot spectrometer, 2 s	(35 – 55)±1 (mixed)	Downtown Toronto fleet, 103 000 plumes
(Wang et al., 2016)	Mobile (in-situ at tailpipe) Mobile (vehicle chase)	AE-51 Aethalometer, 1 s	0.57±1.19 (LDGV, in-situ) 39.5, 313 (2 LDGV, vehicle chase) 1565, 2678 (2 HDDV, vehicle chase)	15 gasoline light duty vehicles, residential (very low traffic) China 2 gasoline vehicles, residential (very low traffic) China 2 diesel trucks, residential (very low traffic) China
(Kelly et al., 2006)	Stationary roadside	Photoacoustic analyzer, 5 s	2400 ± 1300 (HDDV)	Heavy duty diesel trucks (US-Mexico Border region, 2002)

[a]Mean, Median

5. References

Ban-Weiss, G. A., McLaughlin, J. P., Harley, R. A., Lunden, M. M., Kirchstetter, T. W., Kean, A. J., Strawa, A. W., Stevenson, E. D., and Kendall, G. R.: Long-term changes in emissions of nitrogen oxides and particulate matter from on-road gasoline and diesel vehicles, Atmos. Environ., 42, 220-232, 2008.

Dallmann, T. R., DeMartini, S. J., Kirchstetter, T. W., Herndon, S. C., Onasch, T. B., Wood, E. C., and Harley, R. A.: On-road measurement of gas and particle phase pollutant emission factors for individual heavy-duty diesel trucks, Environ. Sci. Technol., 46, 8511-8518, 2012.

Dallmann, T. R., Kirchstetter, T. W., DeMartini, S. J., and Harley, R. A.: Quantifying on-road emissions from gasoline-powered motor vehicles: Accounting for the presence of medium- and heavy-duty diesel trucks, Environ. Sci. Technol., 47, 13873-13881, 2013.

Hudda, N., Fruin, S., Delfino, R. J., and Sioutas, C.: Efficient determination of vehicle emission factors by fuel use category using on-road measurements: downward trends on Los Angeles freight corridor I-710, Atmos. Chem. Phys., 13, 347-357, 2013.

Jiang, M., Marr, L. C., Dunlea, E. J., Herndon, S. C., Jayne, J. T., Kolb, C. E., Knighton, W. B., Rogers, T. M., Zavala, M., Molina, L. T., and Molina, M. J.: Vehicle fleet emissions of black carbon, polycyclic aromatic hydrocarbons, and other pollutants measured by a mobile laboratory in Mexico City, Atmos. Chem. Phys., 5, 3377-3387, 2005.

Kelly, K., Wagner, D., Lighty, J., Quintero Nunez, M., Vazquez, F. A., Collins, K., and Barud-Zubillaga, A.: Black carbon and polycyclic aromatic hydrocarbon emissions from vehicles in the United States-Mexico border region: pilot study, J. Air Waste Manag. Assoc., 56, 285-293, 2006.

Kirchstetter, T. W., Harley, R. A., Kreisberg, N. M., Stolzenburg, M. R., and Hering, S. V.: On-road measurement of fine particle and nitrogen oxide emissions from light- and heavy-duty motor vehicles, Atmos. Environ., 33, 2955-2968, 1999.

Larson, T., Gould, T., Riley, E. A., Austin, E., Fintzi, J., Sheppard, L., Yost, M., and Simpson, C.: Ambient air quality measurements from a continuously moving mobile platform: Estimation of area-wide, fuel-based, mobile source emission factors using absolute principal component scores, Atmos. Environ., 152, 201-211, 2017.

Liggio, J., Gordon, M., Smallwood, G., Li, S.-M., Stroud, C., Staebler, R., Lu, G., Lee, P., Taylor, B., and Brook, J. R.: Are emissions of black carbon from gasoline vehicles underestimated? Insights from near and on-road measurements, Environ. Sci. Technol., 46, 4819-4828, 2012.

Lough, G. C., Schauer, J. J., Lonneman, W. A., and Allen, M. K.: Summer and winter nonmethane hydrocarbon emissions from on-road motor vehicles in the Midwestern United States, J. Air Waste Manag. Assoc., 55, 629-646, 2005.

Miguel, A. H., Kirchstetter, T. W., Harley, R. A., and Hering, S. V.: On-Road Emissions of Particulate Polycyclic Aromatic Hydrocarbons and Black Carbon from Gasoline and Diesel Vehicles, Environ. Sci. Technol., 32, 450-455, 1998.

Park, S. S., Kozawa, K., Fruin, S., Mara, S., Hsu, Y. K., Jakober, C., Winer, A., and Herner, J.: Emission factors for high-emitting vehicles based on on-road measurements of individual vehicle exhaust with a mobile measurement platform, J. Air Waste Manag. Assoc., 61, 1046-1056, 2011.

Roberts, J. M., Veres, P., Warneke, C., Neuman, J. A., Washenfelder, R. A., Brown, S. S., Baasandorj, M., Burkholder, J. B., Burling, I. R., Johnson, T. J., Yokelson, R. J., and de Gouw, J.: Measurement of HONO, HNCO, and other inorganic acids by negative-ion proton-transfer chemical-ionization mass spectrometry (NI-PT-CIMS): application to biomass burning emissions, Atmos. Meas. Tech., 3, 981-990, 2010.

Wang, J. M., Jeong, C. H., Zimmerman, N., Healy, R. M., Wang, D. K., Ke, F., and Evans, G. J.: Plume-based analysis of vehicle fleet air pollutant emissions and the contribution from high emitters, Atmos. Meas. Tech., 8, 3263-3275, 2015.

Wang, Y., Xing, Z., Zhao, S., Zheng, M., Mu, C., and Du, K.: Are emissions of black carbon from gasoline vehicles overestimated? Real-time, in situ measurement of black carbon emission factors, Sci Total Environ, 547, 422-428, 2016.

Westerdahl, D., Wang, X., Pan, X., and Zhang, K. M.: Characterization of on-road vehicle emission factors and microenvironmental air quality in Beijing, China, Atmos. Environ., 43, 697-705, 2009.